Simultaneous Observation of Molecular Tilt and Azimuthal Angle Distributions in Spontaneously Modulated Liquid-Crystalline Langmuir Monolayers

Yuka Tabe, Nan Shen, and Eric Mazur
Harvard University, 9 Oxford St., Cambridge, Massachusetts 02138

Hiroshi Yokoyama
Electrotechnical Laboratory, 1-1-4 Umezono, Tsukuba, Ibaraki 305-8568, Japan
(Received 9 July 1998)

We carried out the first quantitative measurements of correlated modulations of molecular tilt and azimuthal angles in two-dimensional smectic-*C* Langmuir monolayers using simultaneous linear- and circular-polarized reflected light microscopy. For spontaneously formed stripes and higher-order point defects, the tilt angle varies nearly sinusoidally at twice the spatial frequency of the azimuthal rotation. The tilt modulation grows as the second power of the modulation wave number and leads to a large escaped core for the point defect. Our results can be explained by an extended Landau theory of tilted smectics. [S0031-9007(98)08268-4]

PACS numbers: 61.30.Eb, 61.30.Jf, 68.55.–a

Thin films of tilted smectic liquid crystals show a rich variety of spontaneous patterns such as stripes, spirals, and star defects, both in freely suspended films [1–3] and in Langmuir monolayers [4–6]. These films have a thickness of one or several molecular layers and the average direction of the constituent molecules, i.e., the **n** director, is tilted from the layer normal. The projection of the **n** director onto the layer plane gives the **c** director, and the spontaneous patterns observed in tilted smectics are a manifestation of particular modes of spatial modulation of the **c** director. The mechanism of the orientational modulation has attracted much theoretical attention during the last decade [7,8]; the modulation is generally attributed to new elastic free-energy terms, which are forbidden in the bulk but allowed at the interface because of the broken translational and/or mirror symmetry.

For nonchiral systems, in particular, the additional elastic free-energy term is generally written in the phenomenological form, $\lambda\Psi\nabla\cdot\mathbf{c}$, with Ψ a scalar order parameter conjugate to the **c** director gradient and λ a coupling constant. If the coupling is sufficiently strong, this linear term can destabilize uniformly oriented states much like in bulk cholesteric liquid crystals. The phenomenological theory does not specify the origin of the order parameter Ψ. Hinshaw and Petschek [7] adopt the tilt angle itself for Ψ, while Selinger *et al.* [8] consider the more general case of a scalar order parameter. Despite the different origins of Ψ, both models predict virtually indistinguishable azimuthal modulations of the **c** director, in reasonable agreement with experimental observations. However, the two models predict a different behavior for the tilt angle β.

To examine the origin of the spontaneous orientational modulations in smectic-*C* Langmuir monolayers, we simultaneously determined the molecular tilt and azimuthal angle distributions. The monolayer is imaged using a pair of depolarized reflected-light microscopes (DRLM) [9]; see Fig. 1. The DRLM is similar to a Brewster angle microscope but the angle of incidence between the crossed polarizers is much smaller, producing a sharply focused and high-contrast image over the entire field of view. One of the two microscopes (hereafter referred to as C-DRLM) uses circularly polarized light, making it sensitive only to tilt-angle variations. By combining this C-DRLM with a conventional DRLM using linearly polarized light (L-DRLM) we can determine both the tilt angle β of the **n** director from the surface normal and the azimuthal angle α of the director from the incident direction. These angles can be obtained from the linearly and circularly polarized light reflectivities (for derivations, see Ref. [10]):

$$I_L = h_1^2(\cos\alpha - f)^2 \sin^2\alpha \sin^2\beta, \qquad f = \frac{n^2 \tan\theta_t}{n_0^2 \tan\beta}, \tag{1}$$

$$I_C = h_2^2 \sin^4\beta, \tag{2}$$

where n and θ_t are the refractive index and the angle of refraction in water, n_0 is the ordinary refractive index of the uniaxial monolayer, and h_1 and h_2 are the Fresnel factors. Equation (2) shows that C-DRLM selectively images the tilt angle distribution with a rapidly increasing contrast near the normal orientation ($\beta \sim 0$). On the other hand, the L-DRLM image involves both azimuth and tilt angle distributions, but these can readily be separated using the C-DRLM image [11].

The liquid-crystalline monolayer is spread from a 1-mM chloroform solution of 4-octyl-4′-(5-carboxypentamethyleneoxy) azobenzene (8AZ5) on pure water from a milli-*Q* system. In the bulk state, this nonchiral material exhibits a monotropic nematic phase for 140–135 °C, and smectic-*A* phase for 135–130 °C on cooling. In the Langmuir monolayer state, the film shows a 2D smectic-*C* phase at room temperature in the surface pressure of $0 < \pi < 5$ mN/m [6].

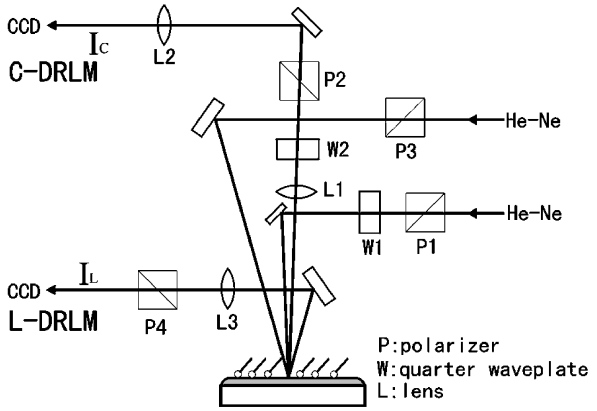

FIG. 1. Experimental setup; 1-mm-diameter beams from two He-Ne lasers for linear-polarized (L-DRLM) and circular-polarized (C-DRLM) depolarized reflected light microscopes overlap on the monolayer. To minimize the effect of oblique incidence [12] the angle of incidence for C-DRLM is 1°. The microscope images are captured by separate CCD cameras.

Figures 2(a) and 2(b) show a typical stripe texture, simultaneously observed by L-DRLM and C-DRLM, respectively. This texture—the most common form of modulation in this 2D smectic-*C* monolayer—develops spontaneously over a period of a few hours after the monolayer is compressed to a continuous smectic-*C* phase. At fixed surface pressure, the stripe width gradually decreases over 12 hours or so until it reaches an apparent equilibrium around a few micrometers. We explored the tilt-azimuth relationship as a function of stripe periodicity during this slow narrowing process.

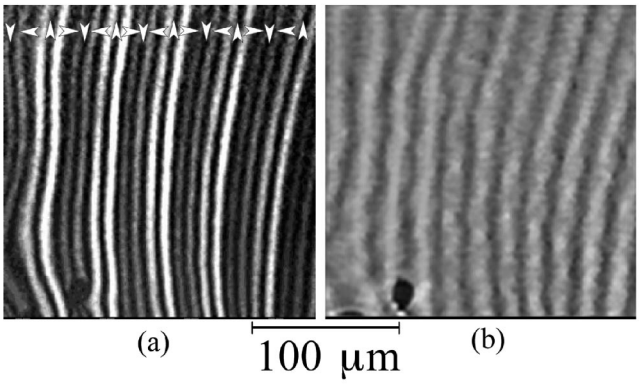

FIG. 2. Stripe structure in 2D smectic-*C* azobenzene Langmuir monolayers: (a) L-DRLM image showing dominantly the azimuthal angle distribution. (b) C-DRLM image showing the tilt angle distribution in the monolayer. The plane of incidence is vertical with the laser incident from the top of the image at angles $\theta_L = 20°$ (L-DRLM) and $\theta_C = 1°$ (C-DRLM). The **c** director (depicted by arrows) completes a full rotation across every four dark bands. The dark bands in (b) correspond to regions of small tilt. The dark circular region at the bottom, probably an entrapped isotropic contaminant, serves as a convenient reference mark in the two images.

Using Eqs. (1) and (2), it follows that, across the stripes shown in Fig. 2(a), the azimuthal angle undergoes a nearly uniform rotation by 2π for every four dark bands with an average tilt $\beta_0 = \pi/4$. The tilt image in Fig. 2(b), on the other hand, shows that the tilt angle exhibits a stripe modulation in phase with the azimuthal stripe. Comparison of the tilt and azimuthal images reveals that the dark bands in Fig. 2(b), which correspond to regions of small tilt, appear twice for each 2π azimuthal rotation. In addition, we find that the tilt angle is smallest where $|\nabla \cdot \mathbf{c}| = 0$ and largest where $|\nabla \cdot \mathbf{c}|$ is maximal. Over the entire range of stripe periodicity we examined, the tilt angle modulation is approximately sinusoidal with a spatial frequency twice that of the azimuthal modulation.

The amplitude of the tilt modulation, however, strongly depends on the stripe width L. This is clearly visible in Fig. 3, which shows the minimum and maximum tilt angles as a function of wave number $q = 2\pi/L$. Near $q = 0$ the modulation amplitude increases quadratically with wave number; accordingly the tilt modulation rapidly diminishes as the stripe widens. The quadratic dependence is consistent with the observation that the tilt modulation has twice the frequency of that of azimuthal angle.

The observed tilt-azimuth modulation can be analyzed in terms of the Landau free-energy expansion introduced by Hinshaw and Petschek [7] and Selinger *et al.* [8] for 2D tilted smectics. These authors attribute the emergence of the modulated patterns to a linear coupling of azimuthal distortion to a scalar order parameter; Hinshaw and Petschek adopt the tilt angle for the order parameter while Selinger *et al.* consider a more general order parameter, ignoring any variation in tilt. In view of the high compressibility of the azobenzene monolayer, we choose the molecular density variation $(\rho - \rho_0)/\rho_0$ as order parameter Ψ and generalize the free energy expansion in the following form:

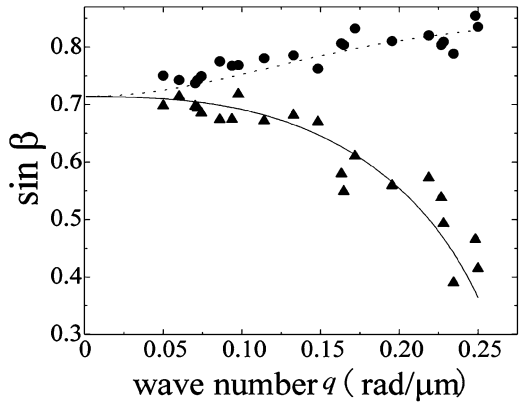

FIG. 3. Wave-number dependence of tilt modulation. Solid circles show the minimum values of the tilt angle given by the intensity of dark bands in the tilt images, and solid triangles give the maximum tilt angle in each bright stripe. Solid and dashed lines are the best-fit theoretical curves calculated from Eq. (3) with parameters $\lambda^2\kappa/W = 8\ \mu\text{m}^2$, $K_1/W = 1.5\ \mu\text{m}^2$, $K_3/W = 2\ \mu\text{m}^2$, $\kappa u = 20\ \mu\text{m}^2$, and $\mu = 0$.

$$F = \int d^2\mathbf{r}\left[\frac{K_1}{2}\sin^2\beta(\nabla\cdot\mathbf{c})^2 + \frac{K_3}{2}\sin^2\beta(\nabla\times\mathbf{c})^2 + \frac{W}{2}(\cos\beta - \cos\beta_0)^2 + (\mu + \lambda\Psi)\sin\beta(\nabla\cdot\mathbf{c}) + \frac{1}{2\kappa}\Psi^2 + \frac{u}{2}(\nabla\Psi)^2\right]. \quad (3)$$

The first three terms are the standard free energy representing the Frank elasticity and tilt anchoring. Added to these are the linear coupling between Ψ and $\sin\beta(\nabla\cdot\mathbf{c})$ with the coefficient λ, the coupling between $\sin\beta$ and $(\nabla\cdot\mathbf{c})$ with μ, and the Landau expansion due to the density variation with κ the compressibility. The direct coupling between the tilt angle and Ψ is omitted because, unlike common Langmuir monolayers, the tilt angle in the azobenzene-derivative monolayers is fixed within a few degrees even under 15% of compression through the smectic-C phase [6,13]; this tilt variation is negligibly small compared with the observed tilt modulation (Fig. 3). Instead of directly solving the Euler equation from Eq. (3), we adopt an ansatz of uniform rotation of $\mathbf{c}$ with wave number q; we thus have $(\nabla\times\mathbf{c})^2 + (\nabla\cdot\mathbf{c})^2 = q^2$. Minimizing F with respect to Ψ and β, and retaining only terms up to order of q^2, yields $\Psi = -\lambda\kappa\sin\beta(\nabla\cdot\mathbf{c})$ and

$$\sin\beta - \sin\beta_0 = -\frac{K_3}{W}\frac{\cos^2\beta_0}{\sin\beta_0}q^2 - \frac{\mu\cot^2\beta_0}{W}(\nabla\cdot\mathbf{c}) + \left(\frac{\lambda^2\kappa}{W} + \frac{K_3 - K_1}{W}\right)\times\frac{\cos^2\beta_0}{\sin\beta_0}(\nabla\cdot\mathbf{c})^2. \quad (4)$$

Because the observed tilt modulation does not contain any appreciable component linear to $\nabla\cdot\mathbf{c}$ for the entire range of observed q, we can conclude that $\mu/W \approx 0$. Substituting this result into Eq. (3) allows us to solve the tilt equation up to even higher orders of q. The solid and dashed lines in Fig. 3 are the theoretical curves thus obtained for the maximum and minimum values of β as a function of q. For $\mu/W = 0$, Eq. (4) shows that the variation of β from β_0 is proportional to q^2 for small q. At high wave numbers, the data points deviate from this q^2 dependence, particularly for the tilt maxima, but the theoretical curves continue to faithfully describe the experimental data (Fig. 3).

Because we observe a minimum in the tilt angle for $\nabla\cdot\mathbf{c} = 0$, it follows from Eq. (4) that $\lambda^2\kappa + K_3 - K_1 > 0$ for $\mu = 0$. Because κ is positive, the larger the linear coupling, the more likely this condition is satisfied. For the theoretical curves in Fig. 3, indeed, the linear coupling is the dominant source of tilt modulation, i.e., $\lambda^2\kappa/|K_3 - K_1| > 10$, while the density variation remains invisibly small with $|\Psi| < 10^{-2}$ even at the largest wave number (using the plausible assumption that $K_3 \sim K_1 \sim 10^{-21}$ J and $\kappa \sim 30$ m^2/J [14]).

In addition to the stripes, the smectic-C azobenzene monolayers sometimes exhibit higher-order orientational point defects which are accidentally formed during the domain coalescence (Fig. 4). The order, or strength, of a point defect is defined by $s = (2\pi)^{-1}\oint d\alpha$, taken counterclockwise along a closed loop around the point defect. In bulk liquid crystals higher-order point defects are seldom observed because the defect energy increases, at least as the square of the defect order s [16].

In the monolayer, however, we observe higher-order point defects for $|s| = \sim 1$–5; the azimuthal images for $+|s|$ and $-|s|$ defects are identical, and therefore do not tell the sign of the defects. In previous work, defects of order up to $|s| = 16$ have been observed [14]. Particularly striking in the tilt images are the dark regions near the

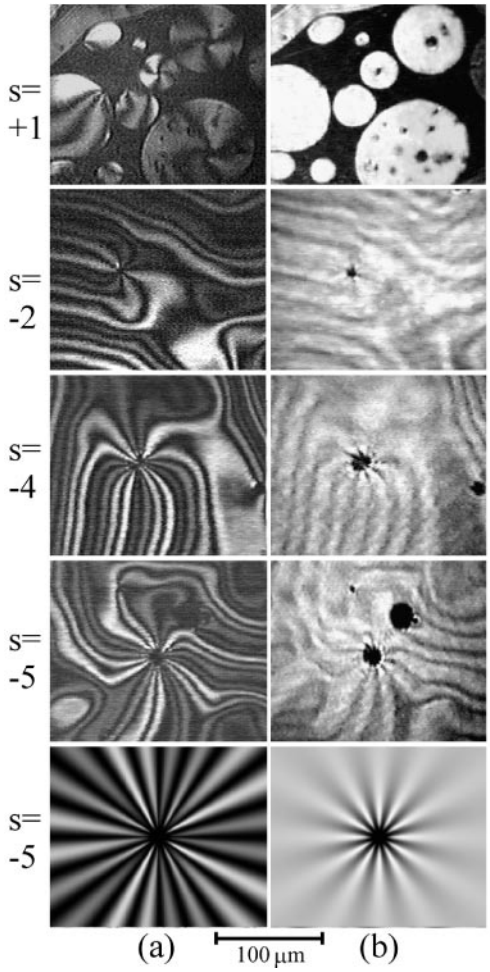

FIG. 4. Higher-order point defects of order s in azobenzene Langmuir monolayers; (a) azimuthal and (b) tilt angle images taken simultaneously. The bottom two images are the simulated $s = -5$ defect images obtained from Eq. (5) with the same parameters as in Fig. 3.

defect center where the molecules are normal to the surface. As the defect order increases, the radius of the dark region increases roughly proportionally to the order $|s|$. This tilt arrangement reduces the Frank elastic energy near the defect point. In analogy to the "escape in the third dimension" at a line defect in 3D nematics [15], the vertical orientation of the molecules at the defect center eliminates the singularity and helps to further reduce the defect energy.

Close observation of the tilt images reveals that the dark regions are not simply round but spiked. The number of dark spikes is equal to $2(|s| + 1)$ for all the higher-order defects we observed, except for the $|s| = 1$ defect, having no dark spikes. To account for these features, we rewrite the Landau free energy in 2D polar coordinates (r, θ) and follow the same procedure as for the stripes. Assuming a homogeneous azimuthal rotation $\alpha = s\theta + \alpha_0$ and postulating a form as $\Psi = \varphi(r) \sin \beta(\nabla \cdot \mathbf{c})$ after the stripe case, we can readily minimize the free energy with respect to φ and β, and obtain

$$\cos \beta = \frac{\cos \beta_0}{1 - G_0 - G_1 \cos 2(s - 1)\theta}, \qquad (5)$$

where G_0 and G_1 are functions of r, which are approximately given by $G_0 \sim [(K_1 + K_3)/(2W)](s/r)^2 - \lambda^2/(2uW)$ and $G_1 \sim [(K_3 - K_1)/(2W)](s/r)^2 + (3\lambda^2)/(2uW)$ near the central dark region with $r/s\sqrt{\kappa u} \ll 1$; $\beta = 0$ when the right-hand side exceeds unity. This expression applies to both positive and negative order defects, and shows that the dark spikes correspond to $\cos 2(s - 1)\theta = 1$ or -1. The number of spikes is therefore equal to $2|s - 1|$. This number is equal to the experimental value $2(|s| + 1)$ only when $s < 0$, indicating that the higher-order point defects in the present monolayer system are preferentially of negative order. Substituting $\beta \sim 0$ in Eq. (5), we find an approximate expression for the average radius of the central dark region $r_0 \sim |s| \times \sqrt{(K_1 + K_3)/[2W(1 - \cos \beta_0) + \lambda^2/u]}$. This expression explains the observed proportionality between the radius of the dark core and the order of defect, and clearly illustrates the competitive roles of Frank elasticity, favoring a larger dark core, and of the linear coupling and anchoring, favoring a smaller core. The bottom two pictures in Fig. 4 show the simulated L-DRLM and C-DRLM images for a point defect of order $s = -5$ obtained from Eq. (5) with the same parameters used for the stripes. The simulated images faithfully reproduce the observed size and shape of the dark region.

The Landau free energy in Eq. (3) cannot explain why the point defects are always negative for $|s| > 1$, because the resultant defect energy, $\sim \pi C s^2[(K_1 + K_3) - \lambda^2/u] \sin \beta_0^2$ with C being a constant of order unity, is identical for $+|s|$ and $-|s|$. Although the present observations do not allow any definitive conclusions, the negative order of the point defects might be due to a boundary contribution to the free energy of the saddle-splay form [17]:

$$F_{24} = -K_{24}^* \int d^2\mathbf{r}\, \nabla \cdot \sin^2 \beta(\mathbf{c}\nabla \cdot \mathbf{c} + \mathbf{c} \times \nabla \times \mathbf{c}), \qquad (6)$$

where K_{24}^* is the *effective* saddle-splay constant including the bulk and the intrinsic boundary contributions. The integral in Eq. (6) can be converted to a line integral along the boundary of the monolayer, yielding $F_{24} = -2\pi S K_{24}^* \sin^2 \beta_0$ where S denotes the sum of defect orders contained within the region. For the stripes, $S = 0$, and so this contribution vanishes. For a region with an sth order defect, however, the integral gives a finite contribution, $-2\pi s K_{24}^* \sin^2 \beta_0$, breaking the symmetry between $|s|$ and $-|s|$ [18]. Adding this contribution to the above defect energy yields an optimal defect order $s_0 = C^{-1} K_{24}^*/[(K_1 + K_3) - \lambda^2/u]$, whereby the defect energy is always negative. For $K_{24}^* < 0$, this result qualitatively explains the preference of negative-order defects and the unusual stability of higher-order defects in the present monolayers.

We are grateful to Professor D. Nelson for valuable discussions. This work was partially supported by the Harvard MRSEC program and the AIST special research fund.

[1] R. B. Meyer and P. S. Pershan, Solid State Commun. **13**, 989 (1973).
[2] S. B. Dierker, R. Pindak, and R. B. Meyer, Phys. Rev. Lett. **56**, 1819 (1986).
[3] J. Maclennan, Europhys. Lett. **13**, 435 (1990).
[4] X. Qiu, J. Ruiz-Garcia, K. J. Stine, C. M. Knobler, and J. V. Selinger, Phys. Rev. Lett. **67**, 703 (1991).
[5] J. Adams, W. Rettig, R. S. Duran, J. Naciri, and R. Shashidhar, J. Phys. Chem. **97**, 2021 (1993).
[6] Y. Tabe and H. Yokoyama, J. Phys. Soc. Jpn. **63**, 2472 (1994); A. Feder, Y. Tabe, and E. Mazur, Phys. Rev. Lett. **79**, 1682 (1997).
[7] G. A. Hinshaw, Jr., and R. G. Petschek, Phys. Rev. A **39**, 5914 (1989).
[8] J. V. Selinger, Z. Wang, R. F. Bruinsma, and C. M. Knobler, Phys. Rev. Lett. **70**, 1139 (1993).
[9] R. Pindak, C. Y. Young, R. B. Meyer, and N. A. Clark, Phys. Rev. Lett. **45**, 1193 (1980).
[10] Y. Tabe and H. Yokoyama, Langmuir **11**, 699 (1995).
[11] A finite f, resulting from the obliquity of illumination [10], breaks the symmetry between $\mathbf{c}$ and $-\mathbf{c}$ (α and $\alpha + \pi$) in L-DRLM images, allowing unique determination of the $\mathbf{c}$ director.
[12] The error due to deviations from normal incidence is $\delta I/I \sim (\Delta\theta_i)^2$ and is here less than 1%.
[13] M. K. Durbin, A. Malik, A. G. Richter, C.-J. Yu, R. Eisenhower, and P. Dutta, Langmuir **14**, 899 (1998).
[14] Y. Tabe, Ph.D. thesis, Tokyo University, 1996; Y. Tabe and H. Yokoyama, Phys. Rev. E (to be published).
[15] P. E. Cladis and M. Kleman, J. Phys. (Paris) **33**, 591 (1972); R. B. Meyer, Philos. Mag. **27**, 405 (1973).
[16] P. G. de Gennes, *The Physics of Liquid Crystals* (Clarendon, Oxford, 1974).
[17] H. Yokoyama, Phys. Rev. E **55**, 2938 (1997).
[18] S. Meiboom, J. P. Sethna, P. W. Anderson, and W. F. Brinkman, Phys. Rev. Lett. **46**, 1216 (1981).